Green Energy and Technology

Lingfeng Wang, Chanan Singh,
and Andrew Kusiak (Eds.)

Wind Power Systems

Applications of Computational Intelligence

With 256 Figures and 63 Tables

Springer

Editors

Dr. Lingfeng Wang
Department of Electrical Engineering
and Computer Science
University of Toledo
Toledo, OH 43606
USA
E-mail: l.f.wang@ieee.org

Dr. Andrew Kusiak
Mechanical and Industrial
Engineering Department
University of Iowa
3131 Seamans Center
Iowa City, IA 52242
USA
E-mail: andrew-kusiak@uiowa.edu

Dr. Chanan Singh
Electrical and Computer
Engineering Department
Texas A&M University
College Station, TX 77843-3128
USA
E-mail: singh@ece.tamu.edu

ISBN 978-3-642-13249-0 e-ISBN 978-3-642-13250-6

Springer Series in Green Energy and Technology ISSN 1865-3529

Library of Congress Control Number: 2010927161

Cover design: WMXDesign, Heidelberg

Printed on acid-free paper

9 8 7 6 5 4 3 2 1

springer.com

Preface

Renewable energy such as wind power has attracted much attention due to its several merits such as environmental friendliness and enhancement of nation's energy security. In recent years, large capacity of wind power is being integrated with conventional power grids. Therefore, it is necessary to address various challenging issues related to wind power systems, which are significantly different from the traditional generation systems. This book is intended as a resource for engineers, practitioners, and decision-makers interested in studying or using the power of computational intelligence based algorithms in handling various important problems in wind power systems at the levels of power generation, transmission, and distribution. This edited book includes the state-of-the-art studies on applications of computational intelligence, including evolutionary computation, neural networks, fuzzy logic, hybrid algorithms, multi-agent reinforcement learning, and several other approaches, to wind power systems. Chapters of original research on computational intelligence applications are included in various research areas including wind turbine control, wind turbine diagnosis, wind farm design, economic dispatch, conductor sizing, reliability analysis, power loss minimization, frequency regulation, and so forth.

In Chapter 1, P. Chen, P. Siano, Z. Chen, et al. present a hybrid optimization method that minimizes the annual system power losses. The method combines the Genetic Algorithm (GA), gradient-based constrained nonlinear optimization algorithm and sequential Monte Carlo simulation (MCS).

In Chapter 2, H. Falaghi and C. Singh propose a probabilistic approach for conductor sizing in electric power distribution systems accounting for wind power generators. The probabilistic evaluation of a solution related to the behavior of the wind power generators is embedded in a GA engine for the search of the optimal conductor planning solutions.

In Chapter 3, A. G. Gonzalez-Rodriguez, J. Serrano-Gonzalez, J. Castro-Mora, et al. discuss global optimization of wind farms based on GA. The proposed method combines a model of wind farm costs based on the life cycle of the facility and a method for searching optimal turbine location and wind farm configuration using GA.

In Chapter 4, M. Ramezani, H. Falaghi, and C. Singh propose three different methods for Capacity Benefit Margin (CBM) evaluation considering wind turbine generator which reflect different objectives. CBM determination is formulated as an optimization problem and Particle Swarm Optimization (PSO) method is used to solve the problem.

In Chapter 5, A. T. Al-Awami and M. A. El-Sharkawi present stochastic dispatch for a power system with both thermal and wind units. Multi-Objective Particle Swarm Optimization (MO-PSO) is employed to obtain the Pareto-front.

In Chapter 6, L. A. Osadciw, Y. Yan, X. Ye, et al. propose an inverse transformation based change detector, called Inverse Diagnostic Curve Detector (IDCD), to track the variation of power curve over time for diagnostics. IDCD is adaptable to different wind turbine types. The dynamic fitting is optimized by a PSO algorithm.

In Chapter 7, L. Yang, G. Y. Yang, Z. Xu, et al. propose the multi-objective optimal controller design of a Doubly Fed Induction Generator (DFIG) based wind turbine system using Differential Evolution (DE).

In Chapter 8, Y. Mishra, S. Mishra, F. Li, et al. discuss various operation modes of the DFIG-based wind farm system. The coordinated tuning of the damping controller to enhance the damping of the oscillatory modes using Bacteria Foraging (BF) technique is presented.

In Chapter 9, H. Bevrani and A. G. Tikdari propose an Artificial Neural Network (ANN) based power system emergency control scheme in the presence of high wind power penetration.

In Chapter 10, B. Singh, S. N. Singh, and E. Kyriakides present efficient control of power-electronic systems used in DFIG-based wind power generation. The conventional proportional-integral (PI) controller is replaced with a nonlinear Adaptive Neuro-Fuzzy Inference System (ANFIS) based controller.

In Chapter 11, H.-S. Ko, K. Y. Lee, and H.-C. Kim present the design of intelligent controllers for a wind-diesel power system equipped with a wind turbine driving an induction generator. The concepts of fuzzy-robust controller and fuzzy-neural hybrid controller are applied to design integrated non-linear controllers to provide control input for excitation system and governor system simultaneously.

In Chapter 12, V. Calderaro, C. Cecati, A. Piccolo, et al. design a sensorless peak power tracking control for maximum wind energy extraction and a voltage control allowing compensation of voltage variations at the wind turbine connection point are proposed. Both the controllers are based on fuzzy logic.

In Chapter 13, S. Mishra, Y. Mishra, F. Li, et al. propose the Tagaki-Sugino (TS) fuzzy controller for the DFIG-based wind generator. The conventional PI control loops for maintaining desired active power and DC capacitor voltage is compared with the TS fuzzy controllers.

In Chapter 14, P. J. Costa, A. S. Carvalho, A. J. Martins, et al. analyze wind power systems and propose a methodology to design fuzzy controllers in order to optimize turbine operation and farm operation.

In Chapter 15, H. Bevrani, F. Daneshfar, and R. Daneshmand present an overview of the key issues on frequency regulation concerning the integration of wind power units into the power systems. An intelligent agent based Load Frequency Control (LFC) using Multi-Agent Reinforcement Learning (MARL) is proposed.

We hope that this edited book has included a bunch of representative applications of computational intelligence techniques in the field of wind power systems. From the collection of these most recent studies, the readers are expected to find some chapters inspiring and useful to their own research. Undoubtedly, in the coming years, there will be increasing complexity and uncertainty in power systems due to the higher degree of wind power penetration. We believe that computational intelligence based methods will be more widely used and play a more important role in this research domain for dealing with various challenging and open-ended problems.

The editors would like to thank all the authors who have contributed their valuable work to this edited book. We are also grateful to all the reviewers who have generously devoted their time to reviewing the manuscripts in their tight schedules. Thanks also go to the Springer staffs who have interacted with us and provided continuous help throughout the production process of this book.

March 2010

L. Wang, Toledo, Ohio
C. Singh, College Station, Texas
A. Kusiak, Iowa City, Iowa

Contents

Optimal Allocation of Power-Electronic Interfaced Wind Turbines Using a Genetic Algorithm – Monte Carlo Hybrid Optimization Method

Peiyuan Chen, Pierluigi Siano, Zhe Chen, and Birgitte Bak-Jensen

Abstract. The increasing amount of wind power integrated to power systems presents a number of challenges to the system operation. One issue related to wind power integration concerns the location and capacities of the wind turbines (WTs) in the network. Although the location of wind turbines is mainly determined by the wind resource and geographic conditions, the location of wind turbines in a power system network may significantly affect the distribution of power flow, power losses, etc. Furthermore, modern WTs with power-electronic interface have the capability of controlling reactive power output, which can enhance the power system security and improve the system steady-state performance by reducing network losses. This chapter presents a hybrid optimization method that minimizes the annual system power losses. The optimization considers a 95%-probability of fulfilling the voltage and current limit requirements. The method combines the Genetic Algorithm (GA), gradient-based constrained nonlinear optimization algorithm and sequential Monte Carlo simulation (MCS). The GA searches for the optimal locations and capacities of WTs. The gradient-based optimization finds the optimal power factor setting of WTs. The sequential MCS takes into account the stochastic behaviour of wind power generation and load. The proposed hybrid optimization method is demonstrated on an 11 kV 69-bus distribution system.

Peiyuan Chen · Zhe Chen · Birgitte Bak-Jensen
Department of Energy Technology, Aalborg University, Pontoppidanstraede 101, Aalborg, Denmark
e-mail: pch@iet.aau.dk, zch@iet.aau.dk, bbj@iet.aau.dk

Pierluigi Siano
Department of Information & Electrical Engineering, University of Salerno, Fisciano (SA), Italy
e-mail: psiano@unisa.it

L. Wang et al. (Eds): *Wind Power Systems*, Green Energy and Technology, pp. 1–23.
springerlink.com

1 Introduction

Wind energy represents a renewable energy resource for electricity generation which contributes to the environment by reducing carbon-dioxide emission. Therefore, many European countries adopt policies to enhance wind energy utilization by means of incentives and financial options.

However, the connection of large amounts of wind turbines (WTs) to distribution systems presents a number of technical challenges to Distribution Network Operators (DNOs) (Masters 2002; Harrison et al. 2008). These challenges, such as steady-state voltage variation, power losses, voltage stability and reliability, are partly due to the mismatch between the location of energy resources and the local network capability of accommodating the new generation. Particularly, the location of WTs is determined by the local wind resources and geographical conditions. However, the capacity of the existing network where the WTs will be connected may not be sufficient to deliver the generated wind power. As a result, network reinforcement is required, which calls for a high capital investment.

System losses, being a major concern for DNOs, may be reduced or increased with the connection of WTs, depending on the locations and capacities of the connected WTs. System losses can be minimized by regulating WTs' power factors or reactive power outputs. This could benefit DNOs by reducing system operation costs without extra investment. Furthermore, DNOs may charge wind power producers for kWh energy flow through their networks by evaluating total network investment and system losses for a time span of 20 years (WTs' life time). Therefore, a reduction in system losses also benefits wind power producers by reducing their connection fee per kWh.

On the basis of the foregoing issues, DNOs would like to explore means to find the optimal locations and capacities of new WTs that can be accommodated within the existing networks, subject to constraints imposed by statutory regulations, equipment specifications and other operational or planning limits. In order to do this, DNOs require a reliable and repeatable method to identify the optimal capacity and location of new Distributed Generation (DG) so that the system power losses are minimized (Harrison et al. 2007a, 2007b, 2008).

A number of techniques were previously proposed to seek the optimal capacities and locations of DG. A common practice is to formulate an optimal power flow problem and to solve for the capacity and location of DG. The objective functions of the optimization formulation include minimizing the system power losses (Rau and Wan 1994; Nara et al. 2001; Kim et al. 2002; Celli et al. 2005), minimizing the investment and operating costs (El-Khaltam et al. 2004), maximizing the net revenue received by DNOs (Harrison 2007b; Piccolo and Siano 2009), maximizing the capacity (Keane and O'Malley 2005; Harrison et al. 2008;) or produced energy from DG (Keane and O'Malley 2007), etc. The constraints of the optimization normally consist of bus voltage limits and line thermal limits. Some also takes into account the short-circuit levels (Vovos et al. 2005) and reliability constraints (Greatbanks et al. 2003). As the DG location is a discrete variable, genetic algorithm (GA) can be used to find the optimal location (Kim et al. 2002;

Celli et al. 2005). Other algorithms such as Tabu search (Nara et al. 2001) can also be used.

Nevertheless, one major limitation in these methods is that the stochastic behaviour of load and wind power generation (WPG) has not been taken into account appropriately. In (Ochoa 2008), typical seasonal load profile is used to account for the seasonal and diurnal variation of load. A one-week time series of WPG has been used to account for its time-varying behavior. However, these are not sufficient to consider the stochastic behavior of load and WPG properly, as a typical daily or weekly curve cannot represent their stochastic behavior throughout a year. More sophisticated stochastic models of load and WPG needs to be adopted.

This chapter proposes a hybrid optimization method that aims at minimizing the total system losses while taking into account the stochastic behaviour of WPG and load during different seasons. The optimization algorithm considers the probability of fulfilling the main constraints, including voltage and current limits. The hybrid optimization method combines the Genetic Algorithm (GA), gradient-based constrained nonlinear optimization and the sequential Monte Carlo simulation (MCS) method. The GA is suitable for finding the optimal capacity and location of WTs as both control variables are integer values. The gradient-based constrained nonlinear optimization is adopted for the optimal power factor setting of WTs as the algorithm usually provides the fastest solution. The sequential MCS method can facilitate the use of time series models and is ideally suited to the analysis of stochastic generation such as wind power (Ubeda and Allan 1992).

The remainder of the chapter is organized as follows. First, a stochastic wind power model is introduced to simulate WPG in a sequential MCS. The cross-correlation of WPG between two wind farms is also considered. Then, the sequential MCS based optimization algorithm is presented for the optimal power factor setting of WTs. Third, the GA for the optimal allocation of WTs is discussed. Following this, the hybrid optimization method is proposed to combine the GA and the sequential MCS based optimization algorithm. Finally, the proposed hybrid optimization method is demonstrated on a 69-bus 11-kV radial distribution system.

2 Stochastic Wind Power Model

This section first introduces a stochastic model of wind power, referred to as the LARIMA model. Then, the cross-correlation modeling of multiple wind farms is presented. Finally, hourly measurements from Nysted offshore wind farm are used to illustrate the stochastic wind power model.

2.1 Single Wind Power Model

WPG shows a strong correlation in time. Such a temporal correlation or autocorrelation requires that realizations of WPG in a time sequence are not independent of each other. In other words, WPG cannot be simply sampled independently from a

probability distribution. The following demonstrates in detail the statistical properties of WPG, followed by the stochastic modeling of WPG (Chen et al. 2009b).

The LARIMA(0,1,1) model developed in (Chen et al. 2009b) for stochastic WPG is briefly summarized as follows. The model was developed on the basis of one-year wind power data measured from the Nysted offshore wind farm with a rated capacity of 165.6 MW. The model is called 'LARIMA' because a limiter is added to a standard autoregressive integrated moving-average (ARIMA) model (Box et al. 1994). In a LARIMA(p, d, q) model, p represents the order of an autoregressive (AR) process, q represents the order of a moving average (MA) process, and d represents the degree of differencing operation. In this case, $p = 0$, $d = 1$, $q = 1$. The model is described by the block diagram shown in Fig. 1. The block diagram consists of a first-order MA model, i.e. the MA(1) model, an integration process, a limiter and a square transformation. The MA(1) model together with the integration process is also referred to as the ARIMA(0,1,1) model. B is a back shifter, similar to a unit delay.

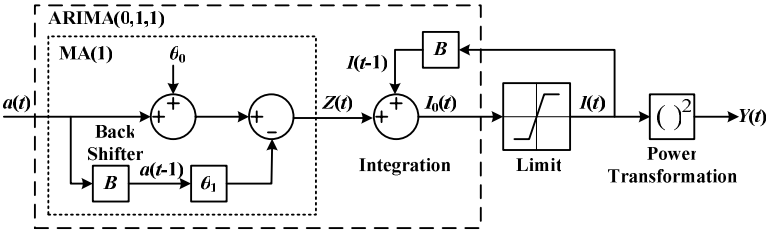

Fig. 1. Block diagram of the LARIMA(0,1,1) model of wind power generation

The LARIMA model can also be described mathematically by Eqs.(1)-(2):

$$Z(t) = \theta_0 + (1 - \theta_1 B)\, a(t) \tag{1}$$

$$Z(t) = I_0(t) - I(t-1) \tag{2}$$

$$I(t) = \begin{cases} \mathrm{I}_{\max}, & I_0(t) > \mathrm{I}_{\max} \\ I_0(t), & \mathrm{I}_{\min} \le I_0(t) \le \mathrm{I}_{\max} \\ \mathrm{I}_{\min}, & I_0(t) < \mathrm{I}_{\min} \end{cases} \tag{3}$$

$$Y(t) = I^2(t) \tag{4}$$

where $\mathrm{I}_{\max}$ and $\mathrm{I}_{\min}$ denote the upper and lower bounds of the square-root of the wind farm power output, respectively. For the considered wind farm, the power output is bounded within [0, 165.6] MW, yielding $\mathrm{I}_{\max} = \sqrt{165.6} = 12.87$ and $\mathrm{I}_{\min} = 0$.

Equation (1) is the MA(1) model; θ_0 is the mean of the MA(1) model; θ_1 determines the temporal correlation (or autocorrelation) of the MA(1) model; $a(t)$ is the Gaussian white noise with variance σ_a. Equation (2) corresponds to one-degree of differencing ($d = 1$), accounting for the time-varying mean of the WPG. Equations (1) and (2) form the ARIMA(0,1,1) model as depicted in Fig. 1. Equation (3) represents the upper and lower limits of the WPG, accounting for the physical limitations of the wind farm. Equation (4) gives the final wind power time series $Y(t)$; the square-transformation accounts for the time-varying variance of the WPG. In summary, the model takes explicitly into account the temporal correlation, the random variation, the physical limitation, and the time-varying mean and variance of the WPG.

The detailed model identification and validation are presented in (Chen et al. 2009b). In brief, the model has in total three parameters (θ_0, θ_1 and σ_a). The model is validated against measurements in terms of temporal correlation and probability distribution in (Chen et al. 2009b). As demonstrated in (Chen et al. 2009b), the model requires much fewer parameters than a discrete Markov model; whereas it shows better performance than the discrete Markov model or an ARMA based model in terms of both the temporal correlation and probability distribution. Therefore, the LARIMA model will be used as the base model for the following correlation modeling.

2.2 Cross-Correlation Model of Wind Power

In the case of several WTs or wind farms in a power system, WPG from these WTs or wind farms may have strong correlations with each other, depending on their geographical locations. In contrast with the autocorrelation of WPG from a single WT or wind farm, this type of correlation is referred to as the cross-correlation of WPG among multiple WTs or wind farms.

In order to account for the cross-correlation of multiple WPGs, the LARIMA model is extended to a vector-LARIMA model. The vector-LARIMA model is established on the theory of vector time series (Wei, 1990), which describes relationships among several time series variables. The following illustration is based on a bivariate time series model. However, a multivariate time series model can be readily derived. Extending the MA(1) model in Fig. 1 to a vector time series model gives the vector-MA(1) model (Wei, 1990)

$$\mathbf{Z}(t) = \boldsymbol{\theta}_\mathbf{0} + \left(\mathbf{U} - \boldsymbol{\theta}_\mathbf{1} B\right)\mathbf{a}(t) \tag{5}$$

In the bivariate case,

$$\mathbf{Z}(t) = \begin{bmatrix} Z_1(t) \\ Z_2(t) \end{bmatrix}, \boldsymbol{\theta}_\mathbf{0} = \begin{bmatrix} \theta_{0,1} \\ \theta_{0,2} \end{bmatrix}, \mathbf{U} = \begin{bmatrix} 1 & 0 \\ 0 & 1 \end{bmatrix}, \boldsymbol{\theta}_1 = \begin{bmatrix} \theta_{11} & \theta_{12} \\ \theta_{21} & \theta_{22} \end{bmatrix}, \mathbf{a}(t) = \begin{bmatrix} a_1(t) \\ a_2(t) \end{bmatrix}$$

where $\boldsymbol{\theta}_\mathbf{0}$ is the mean of the bivariate-MA(1) model. θ_{11} determines the weight of random noise a_1 at time $t - 1$ retained at time t, and contributes to the autocorrelation of Z_1; θ_{22} is interpreted in the same way, but contributes to the autocorrelation

of $Z_2(t)$. θ_{12} determines the weight of a_2 at time $t-1$ retained in Z_1 at time t, and contributes to the cross-correlation between $Z_2(t-1)$ and $Z_1(t)$ at time-lag one; θ_{21} determines the weight of a_1 at time $t-1$ retained in Z_2 at time t, and contributes to the cross-correlation between $Z_1(t-1)$ and $Z_2(t)$ at time-lag one. The white noise $a_1(t)$ and $a_2(t)$ have zero means and a covariance matrix $\mathbf{\Sigma}$.

By also extending Eqs. (2)-(4) to bivariate time series models, a complete bivariate-LARIMA(0,1,1) model is developed. Figure 2 shows the block diagram of the bivariate-LARIMA(0,1,1) model. The model can generate two correlated wind power time series $Y_1(t)$ and $Y_2(t)$. The parameter estimation of the bivariate-LARIMA model given the measured data is discussed in detail in (Chen et al. 2009c).

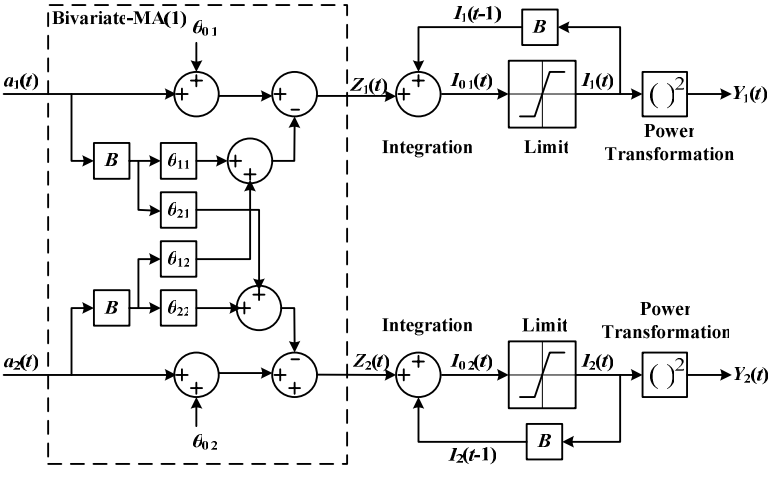

Fig. 2. Block diagram of the bivariate-LARIMA(0,1,1) model of wind power generation

2.3 Bivariate-LARIMA Model for Wind Power Simulation

The following presents a numerical example of the bivariate-LARIMA model based on the wind power data measured from the Nysted offshore wind farm. According to the determined bivariate-LARIMA model, two correlated wind power time series are simulated.

Applying Bivariate-LARIMA Model to Wind Power

Historical wind power data from Part A and Part B of the Nysted offshore wind farm are used for parameter estimations. Part A of the wind farm has the same capacity as Part B, i.e. 82.8 MW. The data are measured on an hourly basis, from January 1 to December 31 in 2005.

In order to account for the seasonal variation, the wind power data are grouped into summer and winter period. For each group of data ($y_1(t)$ and $y_2(t)$), the

square-root and one-degree differencing transformation are applied to obtain two new time series $z_1(t)$ and $z_2(t)$.

$$\begin{cases} z_1(t)=(1-B)\sqrt{y_1(t)} \\ z_2(t)=(1-B)\sqrt{y_2(t)} \end{cases}, \qquad \text{for } t = 1, ..., \text{N}. \tag{6}$$

The sample covariance matrices at time-lag zero, $\underline{\boldsymbol{\Gamma}}(0)$, and that at time-lag one, $\underline{\boldsymbol{\Gamma}}(1)$, for summer and winter period are:

$$\underline{\boldsymbol{\Gamma}}_{\text{sm}}(0) = \begin{bmatrix} 0.70 & 0.63 \\ 0.63 & 0.70 \end{bmatrix}, \underline{\boldsymbol{\Gamma}}_{\text{wt}}(0) = \begin{bmatrix} 0.58 & 0.54 \\ 0.54 & 0.60 \end{bmatrix} \tag{7}$$

$$\underline{\boldsymbol{\Gamma}}_{\text{sm}}(1) = \begin{bmatrix} 0.11 & 0.16 \\ 0.10 & 0.11 \end{bmatrix}, \underline{\boldsymbol{\Gamma}}_{\text{wt}}(1) = \begin{bmatrix} 0.11 & 0.14 \\ 0.11 & 0.11 \end{bmatrix} \tag{8}$$

where subscripts 'sm' denotes summer, and 'wt' denotes winter. In order to understand how strong the autocorrelations and cross-correlations are, the corresponding correlation matrices of Eqs. (7) and (8) need to be calculated (Wei, 1990):

$$\underline{\mathbf{P}}_{\text{sm}}(0) = \underline{\mathbf{P}}_{\text{wt}}(0) = \begin{bmatrix} 1 & 0.91 \\ 0.91 & 1 \end{bmatrix} \tag{9}$$

$$\underline{\mathbf{P}}_{\text{sm}}(1) = \begin{bmatrix} 0.16 & 0.22 \\ 0.15 & 0.16 \end{bmatrix}, \underline{\mathbf{P}}_{\text{wt}}(1) = \begin{bmatrix} 0.19 & 0.24 \\ 0.19 & 0.19 \end{bmatrix} \tag{10}$$

As shown in Eq. (9), the correlation matrix at time-lag zero is the same for summer and winter period. Whereas the correlation matrices at time-lag one, as shown in (10), differ slightly for summer and winter period. The off-diagonal elements of Eq. (9) are the cross-correlation coefficients at time-lag zero (0.91), which are very strong. The diagonal elements of Eq. (10) are the autocorrelation coefficients at time-lag one (0.16 and 0.19), which are rather weak. The off-diagonal elements are the cross-correlation coefficients at time-lag one, which are also very weak. However, these do not necessarily mean that the autocorrelation and cross-correlation at time-lag one of the wind power data $y_1(t)$ and $y_2(t)$ are weak. This is because of the square-root and differencing transformation between $y_i(t)$ and $z_i(t)$ as shown in Eq. (6).

Based on the estimated covariance matrices as in Eqs. (7) and (8), $\boldsymbol{\theta}_1$ and $\boldsymbol{\Sigma}$ for both summer and winter period can be estimated (Chen et al. 2009c):

$$\underline{\boldsymbol{\theta}}_{1,\text{sm}} = \begin{bmatrix} -0.18 & 0.01 \\ -0.46 & 0.25 \end{bmatrix}, \underline{\boldsymbol{\theta}}_{1,\text{wt}} = \begin{bmatrix} -0.11 & -0.10 \\ -0.42 & 0.18 \end{bmatrix} \tag{11}$$

$$\underline{\boldsymbol{\Sigma}}_{\text{sm}} = \begin{bmatrix} 0.68 & 0.61 \\ 0.61 & 0.65 \end{bmatrix}, \underline{\boldsymbol{\Sigma}}_{\text{wt}} = \begin{bmatrix} 0.56 & 0.51 \\ 0.51 & 0.56 \end{bmatrix} \tag{12}$$

Negative elements of $\boldsymbol{\theta}_1$ show a positive correlation and positive elements show a negative correlation. This is because of the minus sign in Eq. (5). Recall that $\boldsymbol{\theta}_1$ determines the weight of random noise at time $t-1$ retained at time t. A small value of $\boldsymbol{\theta}_1$ indicates a weak autocorrelation and cross-correlation of $\mathbf{Z}(t)$ at time-lag one. This is in accordance with the small values of the correlation matrices at time-lag one in Eq. (10). $\boldsymbol{\Sigma}$ is the covariance matrix of the random noise. The corresponding cross-correlation coefficients are also equal to 0.91, both for the summer and winter season. This indicates a strong cross-correlation at time-lag zero, which is in accordance with the large values of correlation matrices at time-lag zero in Eq. (9).

Finally, according to Fig. 2, $\theta_{0,i}$ is adjusted until the sample mean of the simulated time series $Y_i(t)$ coincides with that of the measured time series $y_i(t)$:

$$\underline{\boldsymbol{\theta}}_{0,\mathrm{sm}} = \begin{bmatrix} -0.03 \\ -0.04 \end{bmatrix}, \underline{\boldsymbol{\theta}}_{0,\mathrm{wt}} = \begin{bmatrix} 0.04 \\ 0.05 \end{bmatrix} \tag{13}$$

Wind Power Time Series Simulation

Bivariate wind power time series, $Y_1(t)$ and $Y_2(t)$, are simulated according to Fig. 2. The time-domain plot (only for 2 weeks) and the scatter plot of the two time series are shown in Fig. 3. $Y_1(t)$ is referred to as Wind power A and $Y_2(t)$ is referred to as Wind power B.

In the actual situation, wind may pass through Part A and Part B of the wind farm at the same time, which results in similar WPG from the two parts of the wind farm; whereas wind may pass from Part A to Part B (or from Part B to Part A) of the wind farm, which results in different WPG from the two parts of the wind farm. These two consequences are also observed in the simulated time series in Fig. 3 (a), where Wind power A and Wind power B have identical values during certain periods and discrepancy during other periods. The time-domain plot also shows that Wind power A fluctuates in a very similar way as Wind power B due to their strong cross-correlation. The strong correlation is also observed in the scatter plot in Fig. 3 (b), whose shape tends to follow a straight line. In addition, the two ends of the scatter plot are more condensed than the middle part. This is caused by the upper and lower limits of WPG due to cut-in and rated wind speed.

The sample probability distribution of the sum of Wind power A and Wind power B is shown in Fig. 4 (a). Although not shown here, the sample probability distribution of the model fits well with that of the measurements. For comparison, two wind power time series are simulated independently by using the LARIMA model in Fig. 1 for Part A and Part B of the wind farm without taking into account their cross-correlations. The sample probability distribution of the sum of the two uncorrelated time series is shown in Fig. 4 (b). Evidently, the probability distribution is very different from the one shown in Fig. 4 (a). This indicates the importance of correlation modeling when simulating WPG.

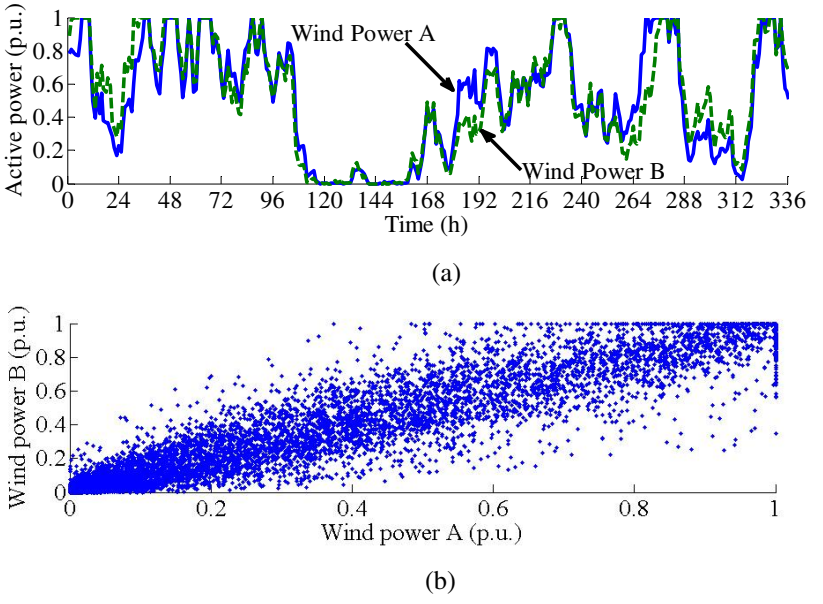

Fig. 3. Wind power A and Wind power B: (a) time-domain plot, and (b) scatter plot

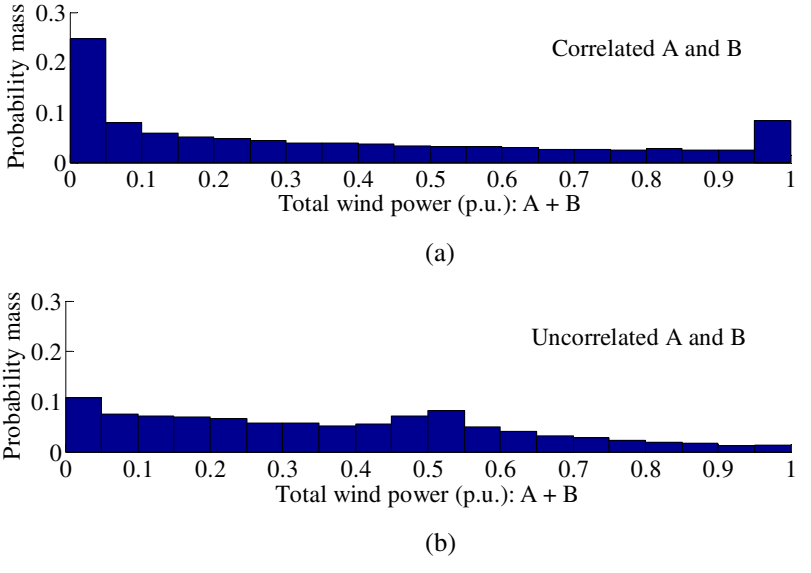

Fig. 4. Effect of cross-correlation on probability distribution of total wind power generation: (a) strong correlation with Eqs. (9) and (10), (b) no correlation

3 Optimization Approaches

During the planning stage of a modern distribution system, utilities are interested in knowing the optimal locations and capacity of WTs in the network so that the total system power losses can be minimized during system operation (Harrison et al. 2007a, 2007b, 2008). In addition, the utilities would like to know if the system power losses can be further reduced by controlling the power factor of WTs. However, the utilities usually confront a dilemma that how the stochastic behavior of wind power can be taken into account in a realistic way. The following demonstrates one solution to the issues addressed above.

The proposed solution combines standard optimization techniques with sequential Monte Carlo simulation (MCS), which is widely accepted as an effective approach to the analysis of stochastic generation (Ubeda and Allan, 1992). The hybrid optimization method is graphically illustrated in Fig. 5. The method consists of four parts: 1) load flow calculation for the evaluation of system steady-state performance, 2) sequential MCS for the probabilistic assessment of load flow results, 3) constrained nonlinear optimization for the optimal power factor setting of WTs, and 4) GA for the optimal allocation of WTs. The following describes the implementation of the hybrid optimization method in detail.

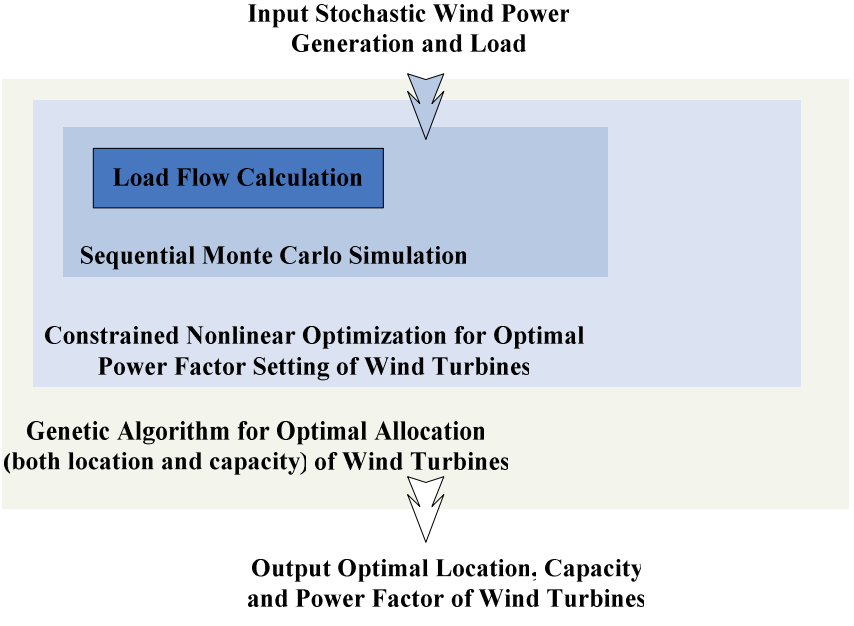

Fig. 5. Scheme of hybrid optimization method

3.1 Optimal Power Factor Setting of Wind Turbines

The constrained nonlinear optimization algorithm aims to minimize total system power losses by controlling the power factor of WTs. The optimization considers the voltage and current limits that are fulfilled at a 95%-probability. As shown in Fig. 5, the optimization requires inputs of total system power losses, bus voltages and line currents from the sequential MCS. The optimization provides outputs of minimum power losses to GA as well as corresponding optimal power factor of WTs. The algorithm for the constrained nonlinear optimization is based on the gradient and Hessian information of the Lagrangian. Mathematically, the objective function of the optimization is to

$$\text{minimize } \overline{\mathrm{P}}_{\mathrm{loss}} = \frac{1}{\mathrm{N}} \sum_{i=1}^{\mathrm{N}} \mathrm{P}_{\mathrm{loss}}(i), \tag{14}$$

where N is the length of a MCS, e.g. 8760 for a evaluation over a year; $\mathrm{P}_{\mathrm{loss}}(i)$ are the total system power losses at i^{th} hour; $\overline{\mathrm{P}}_{\mathrm{loss}}$ are the average system power losses over the study period. The total system losses are calculated by the sequential MCS shown in Fig. 6. The algorithm performs N consecutive load flow calculations in chronological order. The algorithm requires inputs of power factor of WTs, wind power time series and load time series. The algorithm provides outputs of average system power losses $\overline{\mathrm{P}}_{\mathrm{loss}}$ and time series of bus voltages and line currents over the studied period. The optimization is subject to the following constraints:

$$\tan \boldsymbol{\varphi} - \tan(\varphi_{\max}) \le 0, \tag{15}$$

$$-\tan \boldsymbol{\varphi} + \tan(\varphi_{\min}) \le 0, \tag{16}$$

$$\mathbf{F}_{\mathbf{V}}^{-1}(0.975) - \mathrm{V}_{\max} \le 0, \tag{17}$$

$$-\mathbf{F}_{\mathbf{V}}^{-1}(0.025) + \mathrm{V}_{\min} \le 0, \tag{18}$$

$$\mathbf{F}_{\mathbf{I}}^{-1}(0.95) - \mathbf{I}_{\max} \le 0, \tag{19}$$

where $\boldsymbol{\varphi}$ is a vector of power-factor angles of WTs; $\varphi_{\max}$ and $\varphi_{\min}$ are the maximum and minimum power-factor angles, respectively. $\mathbf{P}_{\mathrm{WT}}$ is time series of Wind power A and Wind power B shown in Fig. 3. $\mathbf{P}_{\mathrm{load}}$ and $\mathbf{Q}_{\mathrm{load}}$ are active and reactive load time series, respectively. $\mathrm{V}_{\max}$ is the upper voltage limit and $\mathrm{V}_{\min}$ is the lower voltage limit. $\mathbf{I}_{\max}$ is a vector that contains current limits of all lines/transformers. The following explains Eqs. (17)-(19) in detail.

The inequality constraint of Eq. (17) requires that voltage is below $\mathrm{V}_{\max}$ for minimum 97.5% of the time; and Eqs. (18) requires that voltage is below $\mathrm{V}_{\min}$ for

maximum 2.5% of the time. As a result, the voltage is within $[V_{min}, V_{max}]$ for minimum 95% of the time. This is similar to the requirement set by the EN50160 standard, where 95% of the 10-min mean rms values of the supply voltage shall be within the limits (EN50160, 1999). According to the requirement, 5% voltage violation is tolerated.

$\mathbf{F}^{-1}_{\mathbf{V}}(0.975)$ in Eq. (17) is a vector that contains 97.5%-quantile voltages of all buses. $\mathbf{F}^{-1}_{\mathbf{V}}(0.025)$ in Eq. (18) is a vector that contains 2.5%-quantile voltages of all buses. Both 97.5%-quantile voltages and 2.5%-quantile voltages can be calculated from the voltage time series obtained from the MCS in Fig. 6. A

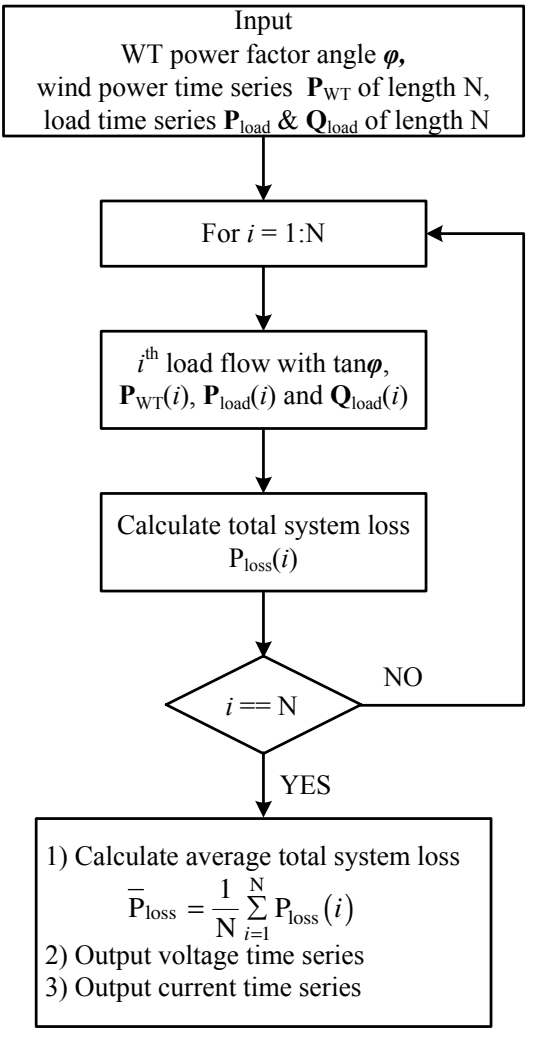

Fig. 6. Flow chart of sequential Monte Carlo simulation based load flow algorithm

97.5%-quantile voltage means that voltage values at a bus are below the quantile voltage for 97.5% of the time. Similar interpretation applies to a 2.5%-quanitle voltage. The two quantiles are also illustrated in a cumulative distribution function shown in the lower plot of Fig. 7. The upper plot of Fig. 7 illustrates the voltage constraints Eqs. (17) and (18) in a probability density function.

The inequality constraint of Eq. (19) requires that current of each line/transformer branch should be below I_{max} for minimum 95% of the time. As a result, overcurrent does not occur for more than 5% of the time. $\mathbf{F}^{-1}_{\mathbf{I}}(0.95)$ is a vector that contains 95%-qauntile current of all branches and is calculated from the current time series obtained from the MCS in Fig. 6. A 95%-quantile current means that current values of a branch are below the quantile current for 95% of the time.

In summary, the proposed optimization algorithm, formulated as Eqs. (14)-(19), searches for optimal power-factor values of WTs in order to minimize the total system losses over a studied period. The algorithm requires that both the statutory voltage requirements and the current requirement should be fulfilled at a 95%-probability.

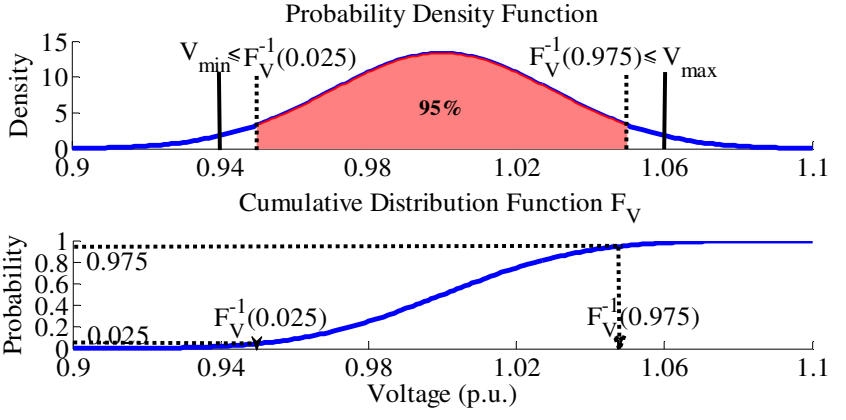

Fig. 7. Interpretation of $F^{-1}{}_V(0.975)$ and $F^{-1}{}_V(0.025)$

3.2 Genetic Algorithm for Optimal Allocation of Wind Turbines

The GA is used in order to select the types and number of WTs to be allocated at each candidate bus. The GA randomly generates the initial population of solutions (individuals) by defining a set of vectors. Each vector, or called a chromosome, has a size $N_e = N_C \times N_T$, where N_C is the number of candidate locations and N_T is the number of defined WT types. This is demonstrated in Fig. 8.

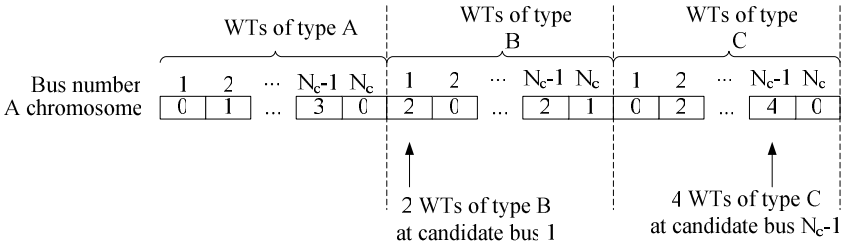

Fig. 8. Schematic of the GA chromosome

As shown in Fig. 8, a chromosome consists of a vector of integers, each of which represents the number of WTs of a given type to be allocated at a candidate bus. For instance, WTs of type A is associated with the first part of the vector with the size of N_C, which is the number of the candidate locations. Each element of this vector is an integer representing the number of WTs of type A connected to the corresponding bus. As such, the locations and types of WTs are expressed as a string of integers.

At each generation of the GA, a new set of improved individuals is created by selecting individuals according to their fitness; the selection mechanism used here is the normalized geometric ranking scheme. After the new population is selected, genetic operators are applied to selected individuals for a discrete number of times. These genetic operators are simple crossover and binary mutation. A simple crossover randomly selects a cut-point dividing each parent into two segments. Then, two segments from different parents are combined to form a new child (individual). A binary mutation changes each of the bits of the parent based on the probability of mutation. An elitism mechanism is also adopted to ensure the best member of the population is not lost. The iteration process continues until one of the stopping criteria is reached.

3.3 Genetic Algorithm - Monte Carlo Hybrid Optimization Method

For each chromosome of the GA, the constrained nonlinear optimization algorithm nested in the GA algorithm computes the fitness function used by the GA and the optimal power factor setting of WTs.

The constrained nonlinear optimization algorithm is based on a sequential MCS, which performs a number of load flow calculations in the chronological order of a year. The sequential MCS generates time series of system power losses, bus voltages and line currents. The system power losses are exported to the constrained nonlinear optimization algorithm as its objective function, with the bus voltages and line currents as its nonlinear constraints. The constrained nonlinear optimization provides outputs of minimum power losses to the GA given a specified number and location of WTs. Consequently, this hybrid method will deliver the best locations as well as the best WT types in the end. The flow chart of the foregoing hybrid optimization method is shown in Fig. 9.

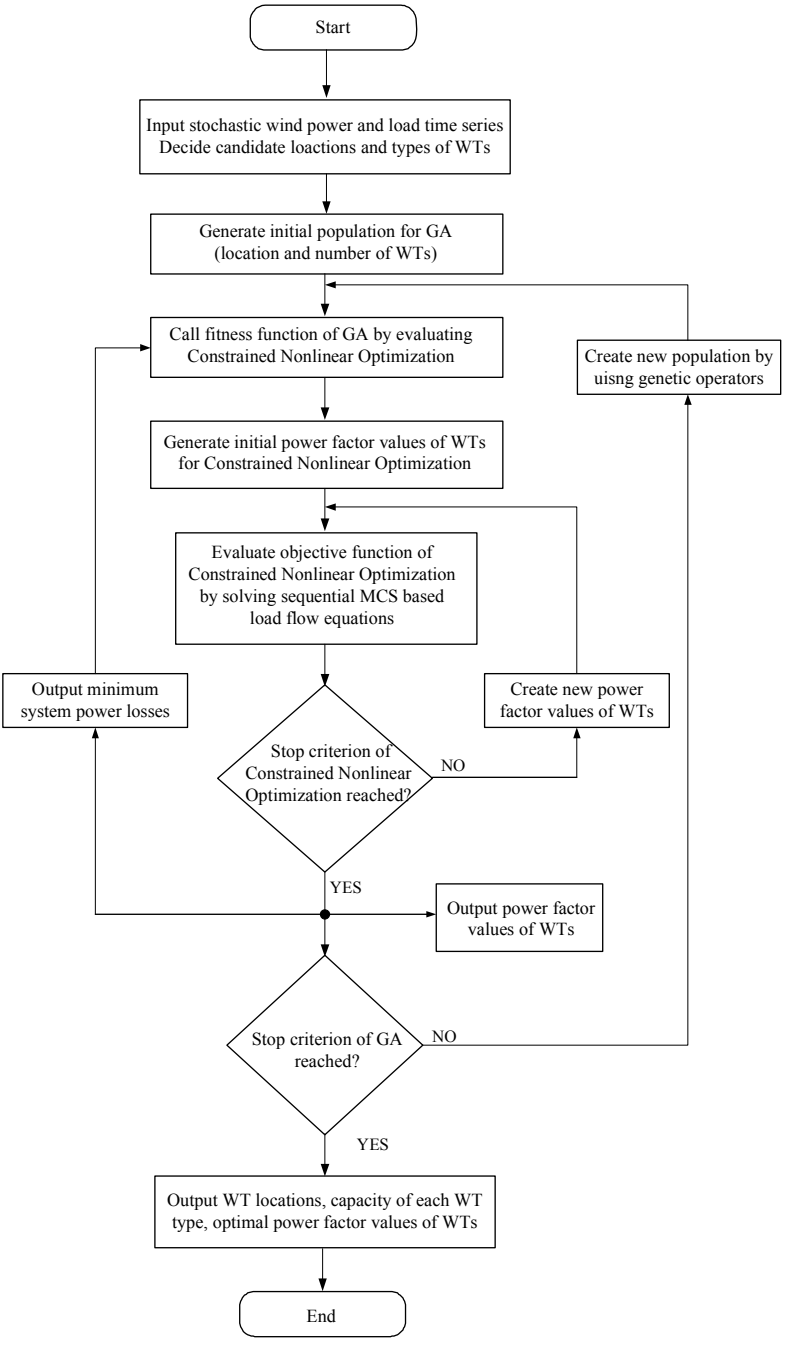

Fig. 9. Flow chart of the Hybrid optimization method

4 Case Study

4.1 System Description

This section describes the distribution system and data that are used to demonstrate the hybrid optimization approach proposed in the previous section for the optimal allocation (both sitting and sizing) and power factor setting of WTs.

69-Bus Distribution System

The 69-bus radial distribution system (Das, 2006) is used as a case network for the simulation studies. The network configuration is shown in Fig. 10 and the network data are provided in (Das, 2006). A 12 MVA 33/11 kV substation transformer is included in the network to connect the four main distribution feeders to the slack bus (bus 1). The upper two feeders are located in area A, and the lower two are located in area B. The 11-kV side of the transformer is denoted as bus 70. The voltage at the 11-kV side is controlled at 1.0167 p.u. by a tap regulator. There are in total 13 tap positions, with maximum six steps above and below the reference position. One tap step adjusts voltage by 0.0167 p.u. The voltage limits of all buses are set to ±6% of the nominal value (11 kV), i.e. V_{max} = 1.06 p.u. and V_{min} = 0.94 p.u. The current limit of all lines is 157A. In this case, the average active power losses of the network without the connection of WTs are 25 kW.

Wind Power and Load Time Series

As shown in Fig. 10, the possible locations of WTs are bus 7, 15, 22 and 29 in area A and bus 38, 43, 50, 56 and 64 in area B. Time series of WPG are simulated from the bivariate-LARIMA model. In particular, WPG from all the four WTs in area A follows the Wind Power A shown in Fig. 3. This assumes a perfect positive linear cross-correlation among the four WTs. A similar assumption is applied to the WTs in area B, where the WPG follows the Wind power B instead. However, the WPG in area A is not linearly correlated with that in area B, but follows the cross-correlation matrices defined in (9) and (10).

In contrast, loads are connected to all the buses from bus 2 to bus 69. The peak load data at each bus are given in (Das, 2006). The total peak load of the network is (2.90 + *j*1.99) MVA. The active load power in area A and in area B follows the Load A and the Load B shown in Fig. 11 (a), respectively. The Load A and Load B are simulated according to the AR(12) based model developed in (Chen et al. 2009a). Load has a strong diurnal and weekly periodicity as shown in Fig. 11 (a). Similar to the WPG in area A, the loads in area A are also assumed to have a perfect positive linear cross-correlation with each other. The same assumption is

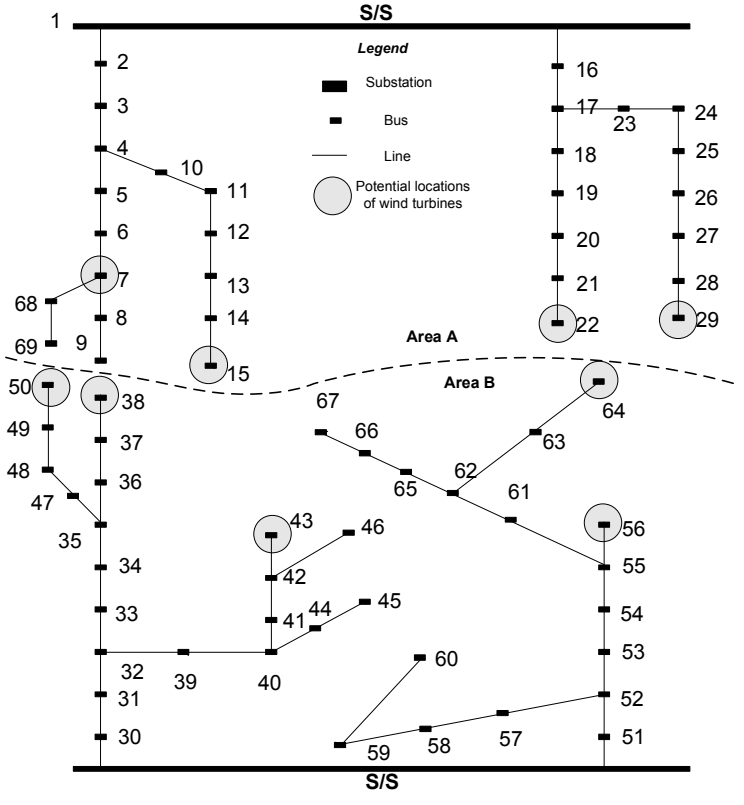

Fig. 10. The 69-bus 11-kV distribution system connected with WTs

applied to the loads in area B. However, the Load A and Load B do not have a perfect linear cross-correlation. Instead, a strong cross-correlation between the Load A and the Load B is present as shown in the scatter plot in Fig. 11 (b). The power factors of the loads are assumed time-invariant as provided in (Das, 2006).

In addition, wind power and load are assumed uncorrelated within summer or winter season. However, wind power and load within a whole year may still be correlated. This is reasonable as the mean values of wind power and load are both lower in summer than in winter. The correlation between wind power and load may be affected due to other factors such as temperature. However, it is rather weak (Papaefthymiou and Kurowicka, 2009) and is not taken into account here.

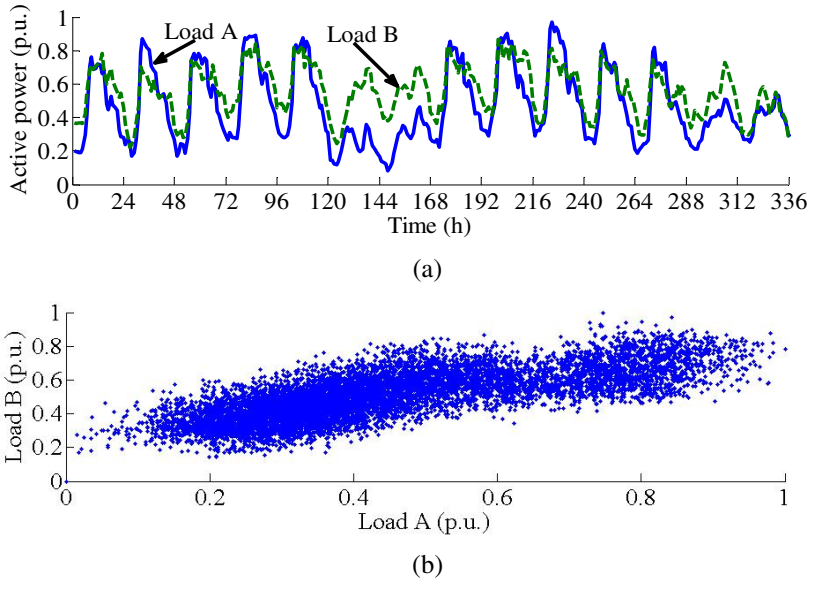

(a)

(b)

Fig. 11. Load A vs. Load B: (a) time-domain plot, (b) scatter plot

4.2 Results

Simulation that uses the hybrid optimization algorithm is carried out on the above-described distribution system with wind power and load time series. It is assumed that WTs of three different capacities are chosen by the DNO. These capacities are 20 kW, 50 kW and 100 kW. Maximum five WTs of each type are allowed at a given location. This requirement may be set by the available land for building WTs. For another distribution network with a different load level, WTs with different capacities may be considered. Consequently, GA is used to search for the optimal number of WTs of each type at the candidate locations. It is also assumed that the power factor is the same for all WTs connected to the same bus.

The entire method has been implemented in the Matlab® environment, incorporating some features of the MATLAB toolbox for GA (MathWorks, 2004). The basic parameters of the GA are summarized as follows. The total control variables are 27 (= 3×9), corresponding to the number of three types of WTs at the nine candidate locations. The population size of each generation is 20. The initial population is generated at random between zero and five. The GA will stop if any of the following conditions is reached: 1) the maximum generation number exceeds 100, 2) there is no improvement in the objective function for 5 consecutive generations, and 3) the cumulative change in the fitness function value over 5 generations is less than 1e-6. Sensitivity analyses have been carried out to consider different values for the GA parameters such as stop criteria, population size and genetic operators. From these analyses, it was shown that the used values guarantee the convergence of the algorithm to a satisfactory solution in this case.

Table 1 lists the initial values of the number of WTs at different buses for the GA. These initial values are the best individual selected from the initial population (with 20 individuals) at the first generation. The corresponding total capacity of the WTs at each bus is also summarized in Table 1. Table 2 lists the optimal numbers of WTs at different locations found by the GA. The total capacity of all the WTs amounts to 1.7 MW, including ten 20-kW WTs, eight 50-kW WTs and eleven 100-kW WTs. As the peak active load of the network is 2.9 MW, the wind power penetration level (i.e. total WT capacity divided by peak active load) in the network is around 59%. In particular, in area A, the total WT capacity is 0.71 MW and the total peak load is 1.17 MW, corresponding to a 61% wind power penetration level. Whereas in area B, the total WT capacity is 0.99 MW and the total peak load is 1.73 MW, corresponding to a 57% wind power penetration level. At bus 22, three 50-kW WTs are determined. In reality, due to the space limitation, DNOs may prefer to connect one 100-kW and one 50-kW WT instead. However, this should be judged by the DNO according to the actual situation.

Table 1. The initial values of the number and power factor of WTs for the hybrid optimization method

Bus no.	20 kW	50 kW	100 kW	Total Capacity (kW)	Power Factor
7	2	4	4	640	1.0
15	2	1	3	390	1.0
22	5	1	0	150	1.0
29	5	3	2	450	1.0
38	3	4	4	660	1.0
43	0	0	2	200	1.0
50	3	5	5	810	1.0
56	4	2	4	580	1.0
64	2	2	2	340	1.0

Table 2. The optimal values of the number and power factor of WTs found by the hybrid optimization method

Bus no.	20 kW	50 kW	100 kW	Total Capacity (kW)	Power Factor
7	1	1	1	170	0.91
15	2	0	1	140	0.92
22	0	3	0	150	0.97
29	0	1	2	250	0.80
38	0	1	1	150	0.89
43	0	0	2	200	0.86
50	2	1	1	190	0.80
56	1	0	2	220	0.80
64	4	1	1	230	0.86

All wind turbines generate reactive power.

Furthermore, the corresponding optimal power factor values of the WTs are also listed in Table 2. The optimal power factor values are found by the gradient-based constrained nonlinear optimization algorithm. The initial power factor values were all set to unity for the optimization algorithm as shown in Table 1. The final optimal power factor values indicate that all the WTs generate reactive power to the network. This is to partly supply the local reactive load in order to minimize the network losses due to the reactive power flow.

Figure 12 shows both the best and mean fitness values found by the GA at each generation. A fitness value of the GA is equal to the average system power losses. Both the best and mean fitness values converge very fast. The GA stops due to the third stop criterion, which indicates that the cumulative change in the fitness function value over five generations is less than 1e-6. The GA obtains an optimal solution after 35 generations. The best fitness value found is around 13.7 kW, which is the minimum average network power loss. Recall that the average network power loss was 25 kW without the connection of WTs. On the basis of the optimal location, capacity and power factor of WTs, the power losses of the network are reduced by more than 45% with the connection of WTs to the network.

Fig. 13 shows the probability density function and cumulative distribution function of the voltage at bus 29, with the given capacity, location and power factor of these WTs. Bus 29 has the largest WT capacity (250 kW). Recall that the voltage constraints require that the 97.5%-quantile voltage should be lower than the maximum voltage (1.06 p.u.) and that the 2.5%-quantile voltage should be higher than the minimum voltage (0.94 p.u.). These two requirements are both fulfilled as shown in Fig. 13. The actual voltage at bus 29 is between 0.96 p.u. and 1.06 p.u., with the mean value of 1.01 p.u.

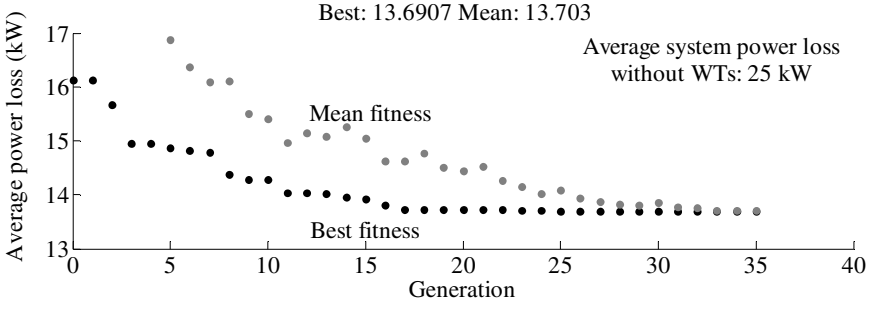

Fig. 12. Best and mean fitness found by the genetic algorithm at each generation

4.3 Discussions

The DNOs' decisions on the optimal locations and capacities of WTs are dependent on the actual or perceived costs or benefits associated with the connection of WTs. In this case, the DNO is interested in reducing the operating costs by simply

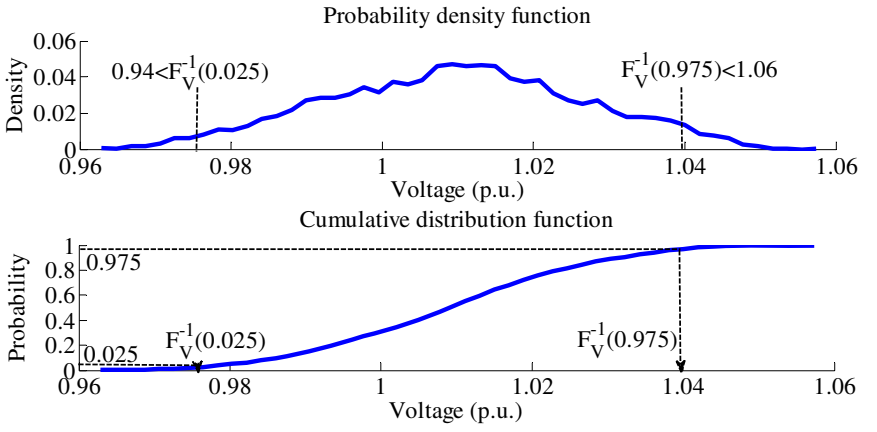

Fig. 13. Probability density function and cumulative distribution function of voltage at bus 29

minimizing network power losses. The proposed method allows the DNO to achieve the power losses minimization by strategically connecting a chosen number and types of WTs, among a large number of potential combinations, to the selected locations in a distribution network.

In order to determine the optimal locations and capacities of WTs, the common practice of DNOs is to assume the worst-case situation of maximum generation at minimum load. This worst-case provides the largest reverse power flows and voltage rises (Harrison et al. 2007a, Harrison et al. 2008), even though the situation may occur at a very low probability or even not occur at all. The proposed hybrid optimization method adopts the sequential MCS instead of the worst-case approach in order to account for the stochastic variation of WPG and load. The proposed method considers not only the probability distribution of WPG and load, but also different possible combinations of WPG from adjacent wind farms and of load from different areas. Consequently, the proposed hybrid method provides a more realistic evaluation of the system and thus a more reliable optimal solution.

In particular, when evaluating system power losses with stochastic WPG, it is important to consider the cross-correlation of WPG between wind farms. An assumption of independence usually leads to an underestimation of the system losses. It is shown in (Chen et al. 2009c) that the system losses may be underestimated by 10% under the assumption of the independence of WPG. On the other hand, the system losses may be overestimated if a perfect positive linear cross-correlation is assumed for wind farms that are distant from each other.

The main drawback of the proposed hybrid optimization algorithm is that the simulation time is very long. This is due to the evaluation of the fitness function which each time calls for a lengthy MCS. However, this drawback can be tolerated as simulation time is not a major concern for long-term system planning. In addition, a more powerful computer may improve the simulation speed to a certain extent.

4 Conclusions

This chapter introduces a hybrid optimization method to find the optimal sitting, sizing and power factor setting of WTs in a distribution system in order to minimize the network power losses. The method combines the GA, gradient-based constrained nonlinear optimization and the sequential MCS method, which takes into account the stochastic behaviour of WPG and load. The optimization algorithm considers a 95%-probability of fulfilling the bus voltage and line/transformer thermal limits. With the proposed optimization algorithm, a significant reduction of system power losses is achieved as a result of the integration of wind power. Therefore, the described hybrid optimization method can be used to assist the network operators to assess the system performance and to plan future integration of WTs in an effective and practical way.

References

Box, G.E.P., Jenkins, G.M., Reinsel, G.C.: Time Series Analysis: Forecasting and Control, 3rd edn. Prentice-Hall, New Jersey (1994)

Celli, G., Ghiani, E., Mocci, S., Pilo, F.: A multiobjective evolutionary algorithm for the sizing and siting of distributed generation. IEEE Trans. Power Systems 20, 750–757 (2005)

Chen, P., Bak-Jensen, B., Chen, Z.: Probabilistic load models for simulating the impact of load management. IEEE PES General Meeting 2009, Calgary, Canada (2009a)

Chen, P., Pedersen, T., Bak-Jensen, B., Chen, Z.: ARIMA-based time series model of stochastic wind power generation. IEEE Trans. Power Systems 25, 667–676 (2010)

Chen, P., Siano, P., Bak-Jensen, B., Chen, Z.: Stochastic optimization of wind turbine power factor using stochastic model of wind power generation. IEEE Trans. Sustainable Energy 1, 19–29 (2010)

Das, D.: A fuzzy multiobjective approach for network reconfiguration of distribution systems. IEEE Trans. Power Del. 21, 202–209 (2006)

El-Khaltam, W., Bhattacharya, K., Hegazy, Y., Salama, M.M.A.: Optimal investment planning for distributed generation in a competitive electricity market. IEEE Trans. Power Systems 19, 1674–1684 (2004)

EN 50160, European standard for voltage Characteristics of electricity supplied by public distribution systems. In: European Committee for Electrotechnical Standardization (CENELEC), Brussels, p. 14 (1999)

Greatbanks, J.A., Popovic, D.H., Begovic, M., Pregelj, A., Green, T.C.: On optimization for security and reliability of power systems with distributed generation. In: Proc. IEEE Power Tech. Conf. (2003)

Harrison, G.P., Piccolo, A., Siano, P., Wallace, A.R.: Distributed Generation Capacity Evaluation Using Combined Genetic Algorithm and OPF. International Journal of Emerging Electric Power Systems 8, 1–13 (2007a)

Harrison, G.P., Piccolo, A., Siano, P., Wallace, A.R.: Exploring the Trade-offs Between Incentives for Distributed Generation Developers and DNOs. IEEE Trans. on Power Systems 22, 821–828 (2007b)